Minería y Geología / v.42/2026/e006 ISSN 1993 8012

ORIGINAL ARTICLE

Rheological Characterization of Carbonate Sludge Slurries (Part II): Evidence of Herschel-Bulkley Behavior

Caracterización reológica de pulpas de cieno carbonatado (Parte II): evidencias del comportamiento de Herschel-Bulkley

Rodney Martínez-Rojas[1*], Arístides Alejandro Legrá-Lobaina[1], Leonel Rafael Garcell-Puyans[2], Gabriel Hernández-Ramírez[3], Héctor Luis Laurencio-Alfonso[4], Jorge Luis Reyes-de la Cruz[1], Gerardo Ruiz-Chavarría[5], Yoalbys Retirado-Mediaceja[1,6]*

[1]Universidad de Moa, Holguín, Cuba

[2]Universidad de Oriente, Santiago, Cuba

[3]Universidad de Holguín, Holguín, Cuba

[4]Universidad Técnica de Cotopaxi, Latacunga, Ecuador

[5]Universidad Nacional Autónoma de México, Ciudad de México, México

[6]Academia de Ciencias de Cuba, Sección de Ciencias Técnicas, La Habana, Cuba

*Corresponding authors: rmartinez@ismm.edu.cu; yretirado@ismm.edu.cu

Abstract

The rheological characterization of carbonate sludge slurries is essential for the design and optimization of pipeline transport systems in the Cuban mining-metallurgical industry. Previous studies have classified these suspensions as Bingham plastics on the basis of limited shear-rate ranges (16 s^{-1}-300 s^{-1}). This research presents an updated rheological characterization using the Herschel-Bulkley model, which accounts for nonlinear post-yield behavior over a broader shear-rate spectrum (10 s^{-1}-650 s^{-1}). An experimental analysis of 63 samples, with solids concentrations (C) between 17 % and 50 %, pH values from 7.71 to 8.52, and polydispersity indices (s) from 0.713 to 0.985, showed that the Herschel-Bulkley model provides a superior fit ($R^2 > 0.99$) compared with the Bingham model ($R^2 \leq 0.98$). The yield stress (τ_0) exhibited an exponential dependence on solids concentration, with a critical transition around 30 %, whereas pH showed an asymptotic influence as it approached the point of zero charge. From a practical standpoint, use of the Bingham model overestimates head loss by 13 % to 41 % (at 30 % and 50 % solids, respectively) relative to the

Herschel-Bulkley model, implying pump oversizing and energy consumption higher than the actual demand. The empirical correlations developed [τ_0, K, n, μ_a = f(C, pH, s)] allow rheological parameters to be estimated with an error below 4.4 % under typical operating conditions at the "Comandante Pedro Sotto Alba" Nickel Company.

Keywords: carbonate sludge slurry, rheological behavior, Bingham model, Herschel-Bulkley model

Abstract

The rheological characterization of carbonate sludge slurries is essential for the design and optimization of pipeline transport systems in the Cuban mining-metallurgical industry. Previous studies have classified these suspensions as Bingham plastics on the basis of limited shear-rate ranges (16 s^{-1}-300 s^{-1}). This research presents an updated rheological characterization using the Herschel-Bulkley model, which accounts for nonlinear post-yield behavior over a broader shear-rate spectrum (10 s^{-1}-650 s^{-1}). An experimental analysis of 63 samples, with solids concentrations (C) between 17 % and 50 %, pH values from 7.71 to 8.52, and polydispersity indices (s) from 0.713 to 0.985, showed that the Herschel-Bulkley model provides a superior fit ($R^2 > 0.99$) compared with the Bingham model ($R^2 \leq 0.98$). The yield stress (τ_0) exhibited an exponential dependence on solids concentration, with a critical transition around 30 %, whereas pH showed an asymptotic influence as it approached the point of zero charge. From a practical standpoint, use of the Bingham model overestimates head loss by 13 % to 41 % (at 30 % and 50 % solids, respectively) relative to the Herschel-Bulkley model, implying pump oversizing and energy consumption higher than the actual demand. The empirical correlations developed [τ_0, K, n, μ_a = f(C, pH, s)] allow rheological parameters to be estimated with an error below 4.4 % under typical operating conditions at the "Comandante Pedro Sotto Alba" Nickel Company.

Keywords: carbonate sludge pulps, rheological behavior, Bingham model, Herschel-Bulkley model

1. INTRODUCTION

Hydraulic transport of mineral suspensions is fundamental in the mining, metallurgical, and chemical industries. Pipeline transport efficiency directly determines the operating costs and economic viability of these processes (Wilson *et al.*, 2020; Visintainer *et al.*, 2023). Accurate knowledge of the rheological behavior of the suspension, that is, how its resistance to flow

varies with shear rate, is essential for the design of pumps, pipelines, and control systems.

At the "Comandante Pedro Sotto Alba" Company (Moa, Cuba), carbonate sludge slurries ($CaCO_3$ > 85 %) are used as neutralizing agents in high-pressure acid leaching. These suspensions are transported by pipeline to the neutralization plant, and their rheology directly affects pump sizing, energy consumption, and operational reliability (Pérez-García *et al.*, 2010; Coussot, 2014). Inaccurate rheological characterization may lead to equipment oversizing or, more critically, to blockage caused by excessive sedimentation and unscheduled shutdowns.

Traditionally, the Bingham model ($\tau = \tau_0 + \mu_p \cdot \dot{\gamma}$) has been the most widely used model to describe concentrated mineral suspensions because of its mathematical simplicity (Slatter, 1997). However, recent research has shown that, for suspensions with broad particle-size distributions and colloidal interactions, post-yield behavior is inherently nonlinear (Mityukov *et al.*, 2021; Derakhshan *et al.*, 2023). The Herschel-Bulkley model ($\tau = \tau_0 + K \cdot \dot{\gamma}^n$) incorporates this nonlinearity through the flow index n, allowing the characterization of shear-thinning fluids (n < 1) or shear-thickening fluids (n > 1) (Chhabra and Richardson, 2008; Coussot, 2014; Carravetta et al., 2020; Wagner *et al.*, 2021). Several studies confirm its superiority over simpler models for concentrated suspensions (Whorton *et al.*, 2025; Yusufi *et al.*, 2025).

Nevertheless, the specific characterization of carbonate sludge slurries from Moa still presents important knowledge gaps. In a previous study, these suspensions were classified as Bingham plastics, but on the basis of narrow experimental ranges (50 s^{-1}-400 s^{-1}) and without adequately considering the influence of pH and polydispersity (Martínez-Rojas and Hernández-Ramírez, 2015). Subsequent studies have revealed systematic deviations from the Bingham model and have emphasized the need for more accurate approaches covering extended operating ranges (Hernández-Ramírez et al., 2016). In particular, the behavior of the slurry at low shear rates ($\dot{\gamma}$ < 50 s^{-1}) and high shear rates ($\dot{\gamma}$ > 400 s^{-1}), as well as the interaction among solids concentration, pH (which varies between 7.7 and 8.5 during normal operation), and the natural polydispersity of the solid phase, remains insufficiently understood.

The objective of this study is to develop an updated rheological characterization of carbonate sludge slurry as a Herschel-Bulkley fluid, overcoming the previous Bingham classification. Specifically, the study aims to: (1) experimentally determine flow curves over a wide shear-rate range

(10 s^{-1}-650 s^{-1}) for solids concentrations (17 %-50 %), pH values (7.71-8.52), and polydispersity indices (0.713-0.985); (2) quantitatively assess the goodness of fit of the Herschel-Bulkley model compared with the Bingham model using rigorous statistical criteria (R^2, AIC, F-test); and (3) implement empirical correlations relating the Herschel-Bulkley parameters (τ_0, K, n) and apparent viscosity (μ_a) to plant-measurable operating variables (C, pH, s).

This characterization provides a robust basis for optimized design of transport systems in the Cuban nickel industry and in similar applications involving carbonate suspensions.

2. MATERIALS AND METHODS

2.1. Characterization of the solid material and slurry

The carbonate sludge slurry comes from biogenic marine sediments from Moa Bay (Holguín, Cuba), composed predominantly of coral-derived $CaCO_3$ (calcite and aragonite) with minor impurities (silica 3 %-5 %, organic matter 1 %-2 %, soluble salts 0.5 %-1.0 %). This material acts as a neutralizing agent in high-pressure acid leaching at the "Comandante Pedro Sotto Alba" Company, raising the liquor pH from 1.4-1.6 to the optimum range of 2.4-2.6 for selective nickel and cobalt precipitation (Castellanos *et al.*, 2011). The slurry is processed by wet grinding, classification, and washing to reduce chlorides below 600 ppm, a critical requirement for corrosion prevention (Estrada *et al.*, 2007; Hernández-Rodríguez *et al.*, 2015). It is then thickened to 35 %-45 % solids and pumped approximately 5 km through a steel pipeline to the company's Neutralization Plant. Table 1 compares the physicochemical characteristics of the slurry according to process specifications and actual measurements.

Table 1. Physicochemical characteristics of carbonate sludge slurries

Parameter	Unit	Process specification	Measured values
Slurry density	kg/m³	1320-1400	1310-1412
Solid density	kg/m³	2410-2580	2476
Solids concentration	%	35-48	17-50
Temperature	°C	28.7	27.3
Calcium carbonate	%	≥87	85.5-90.3
pH	…	8-9	7.71-8.52
Chloride content	ppm	500-600	397-503

2.2. Operating variables influencing the rheological behavior of the slurry

2.2.1. Solids concentration (C)

Solids concentration is a primary variable influencing suspension rheology: as the number of particles increases, interparticle interactions intensify, forming percolated networks that confer viscoplastic characteristics once the percolation threshold is exceeded (Ness *et al.*, 2022). For this research, concentrations covering the industrial operating range were selected (17.41 %; 23.86 %; 30.16 %; 35.31 %; 39.90 %; 45.60 %; and 49.86 %), from the dilute regime to the highly concentrated regime. The mass concentration (C) was determined using Equation 1, according to Martínez-Rojas *et al.* (2026).

$$C = \frac{m_s}{m_s + m_w} \times 100 \quad (1)$$

where m_s (g) is the mass of solid particles and m_v (g) is the mass of water.

2.2.2. Degree of alkalinity (pH)

The pH controls the surface charge density of particles through protonation/deprotonation reactions at the solid-liquid interface. For calcium carbonate, surface charge arises from ionic equilibria (Ca^{2+}, CO_3^{2-}, H^+, OH^-). The point of zero charge (p.z.c.) - the pH at which the net surface charge is zero - determines colloidal stability (Hunter, 2001). Below the p.z.c., the surface is positive (protonation); above it, the surface is negative (deprotonation). Maximum attraction and flocculation occur near the p.z.c., where electrostatic repulsion is minimized, thereby increasing yield stress. Based on historical plant data, three pH values were selected: 7.71 (below the p.z.c.), 8.14 (near it), and 8.52 (above it). Following standardized procedures (Leong *et al.*, 1991), adjustment was performed with HNO_3 (0.5 mol/L) or KOH (0.15 mol/L), keeping the solids concentration constant within each series.

2.2.3. Polydispersity index (s)

Particle-size distribution affects suspension rheology through its influence on packing efficiency, interparticle spacing, and force-chain networks (Pérez-García and Garcell-Puyáns, 2006, 2017; Pérez-García *et al.*, 2010). Polydisperse systems exhibit lower viscosity than monodisperse systems at equivalent concentrations because smaller particles fill the voids between larger particles, improving packing. The polydispersity index (s) was determined using the particle-size model of Pérez-García (2010), Equation 2, which has been validated for lateritic and carbonate suspensions (Hernández-Ramírez *et al.*, 2016):

$$Y_N = \left(\frac{D_N}{(1-B_N)D_N + B_N}\right)^s \quad (2)$$

where $D_n = D/D_{50}$ (μm) is the normalized diameter, $Y_n = Y/Y_{50}$ (%) is the normalized cumulative fraction, D_{50} is the median diameter, and B_n is a free parameter obtained by nonlinear regression. The polydispersity index (s) quantifies distribution heterogeneity: values close to zero ($s < 0.05$) indicate nearly monodisperse distributions, whereas $s > 0.7$ denotes highly polydisperse systems (ISO-22412, 2008). The distributions were measured with an "Analysette 22 COMPACT" laser analyzer (Fritsch GmbH, Germany; range 0.3 μm-300 μm) according to ISO 13320:2020, using laser diffraction (635 nm diode, <1 mW). Measurements were performed in triplicate under mechanical stirring, ensuring repeatability (RSD <3 % for D_{50}).

2.3. Sample preparation and experimental design

2.3.1. Sample collection

Samples were collected from three points in the slurry preparation plant: TK1 (first settler, 15 %-25 % solids), TK2 (second settler, 25 %-35 % solids), and TK3 (collector tank, 35 %-45 % solids). Three composite samples were obtained from each location (MC1-MC9), with initial solids concentrations between 18.51 % and 46.54 % (Table 2).

Table 2. Initial solids concentrations of the collected samples

Sampling point	Sample	Solids concentration (%)
TK1	MC1	18.51
TK1	MC2	24.37
TK1	MC3	21.58
TK2	MC4	33.61
TK2	MC5	38.13
TK2	MC6	36.23
TK3	MC7	38.94
TK3	MC8	41.28
TK3	MC9	46.54

2.3.2. Sample preparation for target concentrations

To reach the desired experimental concentrations (17 %, 24 %, 30 %, 35 %, 40 %, 45 %, and 50 %), the initial samples were modified by sedimentation and dilution. The 50 % concentration was obtained from sample MC9 after 30 min of sedimentation and supernatant removal until 49.86 % was reached. Samples MC8 and MC9 were concentrated or diluted to reach 40 %-45 %; MC6 (36.23 % original) was diluted to 30 %-35 %; and MC1-MC4 were diluted to 17 %-24 %. Each target concentration was prepared in triplicate,

producing 21 primary samples (seven concentrations × three replicates), in accordance with protocols recommending repeated measurements to ensure reproducibility (ASTM D2196). For each primary sample, the pH was adjusted to three levels (7.71, 8.14, and 8.52) with HNO_3 or KOH, a standard procedure in mineral suspensions (Leong *et al.*, 1991), resulting in 63 experimental samples. The polydispersity index (s) was measured after pH adjustment.

2.4. Measurement of rheological properties

2.4.1. Equipment

Rheological measurements were performed with two complementary rotational viscometers. The first was a HAAKE VT 550 rheometer (Thermo Fisher Scientific, Germany), a controlled-shear-rate Searle-type instrument with SV DIN coaxial cylinders, used for shear rates from 10 s^{-1} to 650 s^{-1} (the main range of industrial interest). The sequence used a decreasing angular-velocity ramp with automatic conversion of torque and speed into shear stress and shear rate. The second was a Brookfield DVELV viscometer (AMETEK, USA), used at low speeds (0.06 s^{-1}-20 s^{-1}) to evaluate yield stress and wall-slip effects. Because the smooth surface of the SV DIN probe may promote slip at low stresses, comparative measurements were performed with rough surfaces (spindles covered with sandpaper) to quantify this phenomenon (Hopmann *et al.*, 2025), whose quantification is essential for accurate characterization of yield-stress fluids (Geri *et al.*, 2024).

2.4.2. Measurement protocol

The measurement protocol followed the recommendations for concentrated suspensions. Temperature was controlled within ±0.5 °C to minimize viscosity effects. Nine shear rates were used in decreasing order to mitigate sedimentation during measurement (ASTM D2196-10). To ensure repeatability, three replicates were performed per point (ASTM D2196), increasing to ten replicates at low shear rates ($\dot{\gamma} < 20\ s^{-1}$) owing to the greater variability in this region, consistent with the need for accuracy in non-Newtonian fluids.

2.4.3. Evaluation of wall slip

To evaluate wall-slip effects, comparative measurements were performed using smooth and rough spindles. For rough-surface measurements, sandpaper (P120 grit) was attached to the spindle, increasing the effective radius by $\Delta r = 0.45$ mm, an inexpensive and effective procedure for suppressing wall slip (Minale, 2013; Carotenuto *et al.*, 2015; Abbasi Moud *et al.*, 2021). The use of rough surfaces is particularly relevant in mineral suspensions, where slip is related to thixotropic phenomena and depends

critically on surface roughness (Piette *et al.*, 2024). Shear-stress correction was applied according to Equation 3, considering the increase in effective radius caused by the sandpaper layer.

$$\tau = \frac{M}{2\pi H(r+\Delta r)^2} = \frac{M}{2\pi H r^2} \cdot \frac{1}{\left(1+\Delta r/r\right)^2} \quad (3)$$

where M (Nmm) is the measured torque, H (mm) is the spindle height, and r (mm) is the nominal spindle radius.

2.5. Fitting of the Herschel-Bulkley model

To fit the Herschel-Bulkley model ($\tau = \tau_0 + K\dot{\gamma}^n$) to the ordered pairs ($\dot{\gamma}_i$, τ_i), an iterative optimization procedure was followed based on maximizing the linear correlation coefficient through model linearization after fixing the flow index n. With n fixed, the model is linearized as $\tau = \tau_0 + K \cdot X$ with $X = \dot{\gamma}^n$, yielding a correlation coefficient r(n) that depends on n. The best fit corresponds to the value of n that maximizes r(n), that is, the value closest to 1. For the data in this study, when r(n) was calculated for n in [0, 1] with a step $\delta = 0.001$, r(n) showed a maximum within that interval. The iterative procedure consists of: (1) calculating r(n) in [0, 1] with a step of 0.001, obtaining $r_0$max at $n = n_0$; (2) redefining the interval as [n_0 - 0.001, n_0 + 0.001] with step $\delta_1 = 10^{-6}$; (3) obtaining $r_1$max at $n = n_1$; and (4) repeating until the difference between two consecutive rmax values is less than 10^{-9}. The final value of n_1 determines τ_0 and K by linear regression on the transformed model. Because the Herschel-Bulkley model is nonlinear in its parameters, the least-squares method cannot be applied directly (Mullineux, 2008).

The apparent viscosity at a specific shear rate was calculated using Equation 4:

$$\mu_a(\dot{\gamma}) = \frac{\tau}{\dot{\gamma}} = \frac{\tau_0 + K\dot{\gamma}^n}{\dot{\gamma}} = \frac{\tau_0}{\dot{\gamma}} + K\dot{\gamma}^{n-1} \quad (4)$$

where τ_0 (Pa), K (Pa·s^n), and n (dimensionless) are the Herschel-Bulkley parameters. For industrial applications, the characteristic shear rate $\dot{\gamma} = 231\ s^{-1}$ (actual value of the production process) was selected, corresponding to the average flow in the transport pipelines.

2.6. Statistical analysis and model validation

2.6.1. Goodness-of-fit criteria

For each fitted model, the following statistical indicators were evaluated: coefficient of determination (R^2), standard error (E), and residual analysis.

2.6.2. Comparison with the Bingham model

To quantitatively justify the transition from the Bingham model to the Herschel-Bulkley model, both models were fitted to each flow curve and compared using two criteria. The first was the Akaike information criterion (AIC = 2p + n·ln(RSS/n)), where p is the number of parameters, n is the number of points, and RSS is the residual sum of squares; lower AIC values indicate a better fit by penalizing additional parameters. The second criterion was an F-test for nested models, since Bingham is a particular case of Herschel-Bulkley (when n = 1), to determine whether the additional parameter n significantly improves the fit.

2.6.3. Empirical correlations

For engineering applications, empirical correlations were developed (Martínez-Rojas *et al.*, 2026) relating the Herschel-Bulkley parameters (τ_0, K, n) to operating variables (solids concentration C, pH, and polydispersity index s) by multiple linear and nonlinear regression, according to the general form P = f(C, pH, s), where P represents τ_0, K, or n. In the present work, these correlations are used to estimate the rheological parameters; additionally, the apparent viscosity is obtained from these parameters and the characteristic shear rate of the process.

3. RESULTS AND DISCUSSION

3.1. Particle-size distribution and polydispersity

Figure 1 shows the cumulative particle-size distributions for three representative samples (MC2, MC4, and MC8). All samples exhibit similar features: predominantly particles smaller than 100 μm, with median diameters (D_{50}) between 5.2 μm and 34.3 μm. The distributions indicate approximately 50 % clay-sized particles (<3.9 μm), 40 % silt (3.9-62.5 μm), and 10 % fine sand (62.5-100 μm).

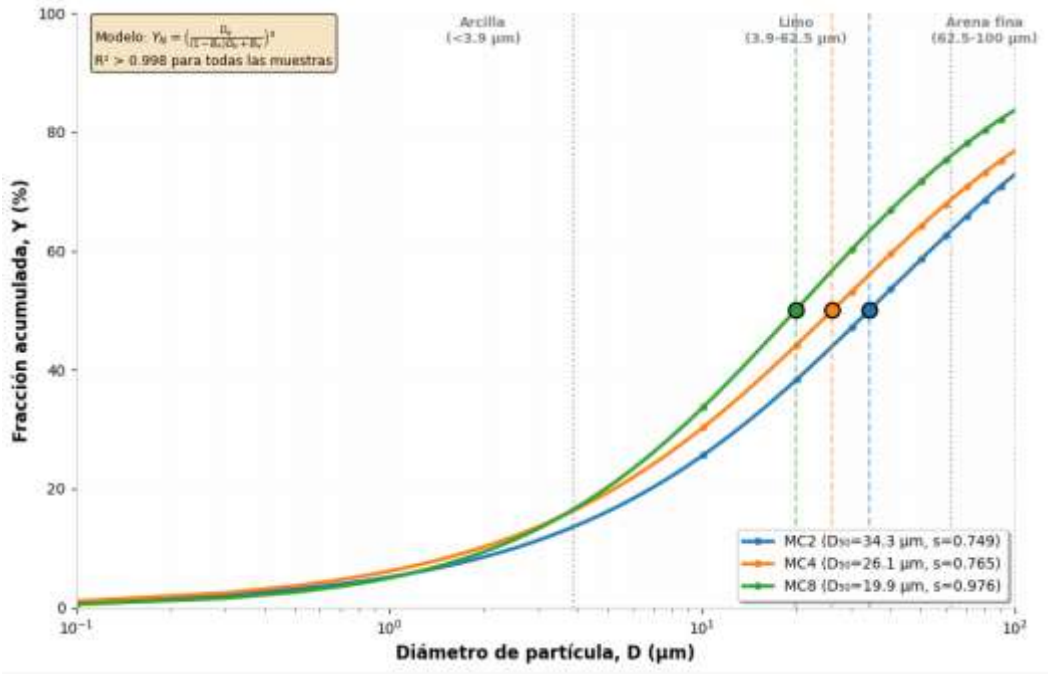


Figure 1. Cumulative particle-size distributions for carbonate sludge slurry samples (MC2, MC4, and MC8).

The polydispersity index (s) ranged from 0.749 to 0.976 (Table 3), values that, according to ISO 22412 (2008), characterize highly polydisperse systems (s > 0.7). Sample MC8 (s = 0.976) showed the narrowest distribution (approaching monodispersity), whereas MC2 (s = 0.749) exhibited the broadest distribution. This variation affects rheological behavior through packing efficiency and interparticle interactions (Pérez-García *et al.*, 2010; Boyer *et al.*, 2011). The particle-size model proposed by these authors showed an excellent fit ($R^2 \geq 0.998$), validating its applicability. The parameter s effectively captures the distribution characteristics that affect flow properties.

Table 3. Particle-size model parameters and polydispersity indices

Sample	D_{50} (µm)	B_N	s	R^2
MC2	34.255	0.601	0.749	0.998
MC4	26.111	0.582	0.765	0.998
MC8	19.904	0.512	0.976	0.999

3.2. Flow curves and rheological behavior

3.2.1. Influence of solids concentration

Figure 2 shows the flow curves (τ vs. γ̇) for carbonate sludge slurries at seven solids concentrations (17 %-50 %), constant pH of 8.14, and polydispersity indices varying according to the sample.

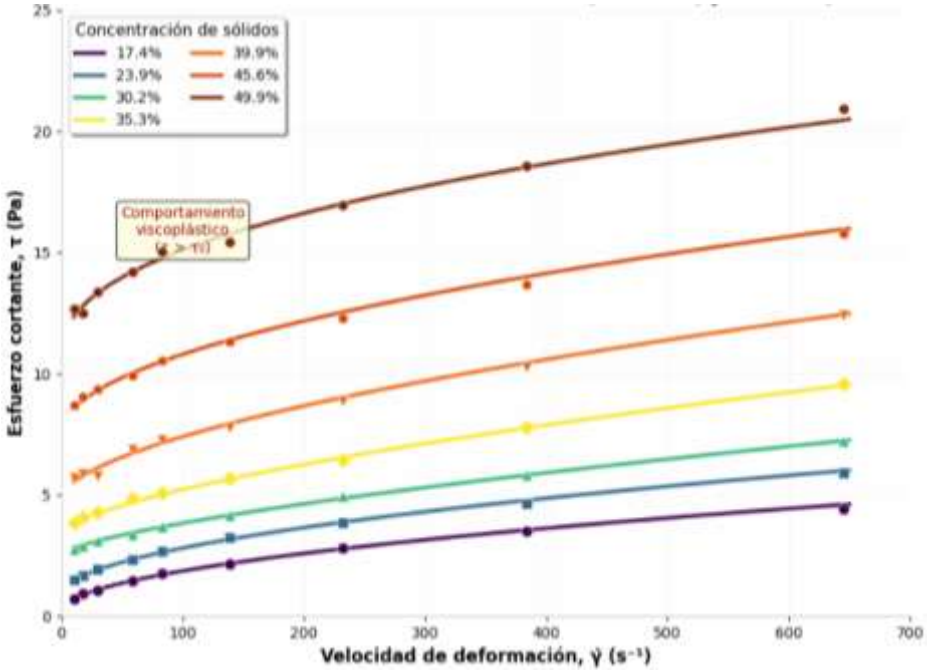


Figure 2. Flow curves of carbonate sludge slurries at different solids concentrations (T = 28 °C, pH = 8.14). Continuous lines represent Herschel-Bulkley fits.

All curves exhibit viscoplastic behavior: a yield stress that must be exceeded to initiate flow, followed by a nonlinear increase in stress with shear rate. At a fixed shear rate, shear stress increases monotonically with solids concentration, reflecting the intensification of interparticle interactions (Boyer *et al.*, 2011).

At low concentrations (17 %-24 %), the curves show modest yield stresses (τ_0 < 1.6 Pa) and nearly linear post-yield behavior (Table 4). When the concentration increases to 30 %-35 %, the yield stress increases substantially (τ_0 = 2.3 Pa-3.5 Pa) and slight curvature appears. At the highest concentrations (40 %-50 %), the yield stress rises sharply (τ_0 = 5.7 Pa-12.8 Pa), with marked nonlinearity and a significant decrease in the flow index n.

Table 4. Herschel-Bulkley parameters for carbonate sludge slurries at different solids concentrations (pH = 8.14)

C (%)	τ_0 (Pa)	K (Pa·s^n)	n	R^2
17.41	0.2235	0.1439	0.5276	0.9981
23.86	0.8877	0.1703	0.5255	0.9962
30.16	2.5355	0.0537	0.6909	0.9968
35.31	3.3973	0.0911	0.6501	0.9983
39.90	4.8807	0.1660	0.5902	0.9963
45.60	7.5726	0.3038	0.5127	0.9974
49.86	10.7022	0.6127	0.4277	0.9958

The correlation coefficients (R^2 > 0.995 for all samples) show that the Herschel-Bulkley model describes the experimental data excellently over the entire concentration range. The flow index n decreases from approximately 0.527 at low concentrations to 0.427 at 50 %, indicating increasingly pronounced viscoplastic behavior as concentration increases (Boyer et al., 2011).

Figure 3 shows the dependence of yield stress on solids concentration in semilogarithmic coordinates, revealing two distinct regimes. In Regime I (C < 30 %), τ_0 increases moderately with concentration, with approximately linear behavior. In Regime II (C > 30 %), τ_0 exhibits exponential growth, where small increases in concentration produce a substantial increase in yield stress.

This transition around 30 % solids corresponds to the formation of a percolated particle network spanning the entire suspension volume. Below this critical concentration, particles interact mainly through hydrodynamic forces without forming a continuous network. Above the percolation threshold, interparticle contacts create a space-filling structure that imparts significant yield stress and viscoplastic characteristics (Boyer *et al.*, 2011).

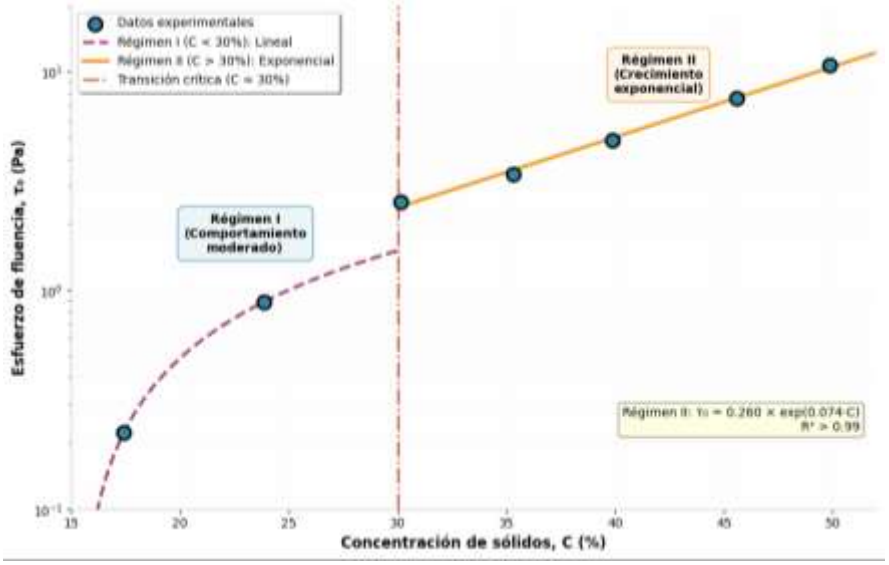


Figure 3. Yield stress τ_0 as a function of solids concentration C (semilogarithmic scale). The dashed vertical line indicates the transition around 30 % solids.

3.2.2. Influence of pH

Figure 4 shows flow curves for carbonate sludge slurries at three pH values (7.71, 8.14, and 8.52), with constant solids concentration (C = 40 %) and similar polydispersity (s ≈ 0.85).

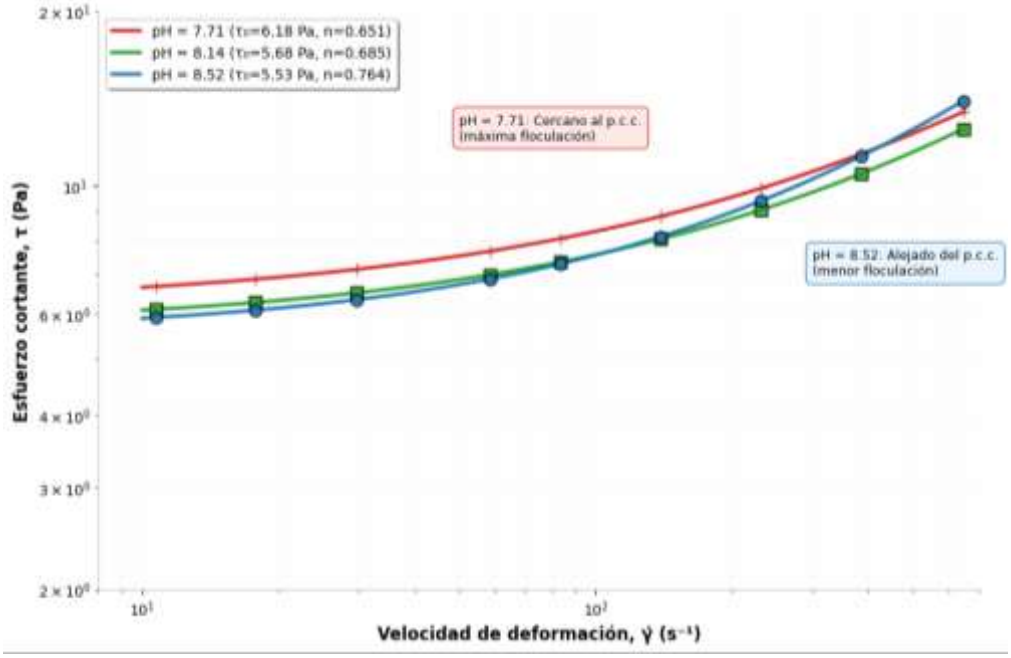


Figure 4. Flow curves at different pH values (C = 40 %, T = 28 °C). Continuous lines: Herschel-Bulkley fits.

The pH exerts a systematic influence on rheological behavior (Table 5): at a fixed shear rate, shear stress decreases as pH increases. The effect is more pronounced at low shear rates and near the yield point, where interparticle forces dominate flow (Cardero and Garcell, 2016).

Table 5. Herschel-Bulkley parameters at different pH values (C = 40 %)

pH	τ_0 (Pa)	K (Pa·s^n)	n	R^2
7.71	6.1777	0.1068	0.6510	0.9981
8.14	5.6827	0.0811	0.6850	0.9984
8.52	5.5318	0.0603	0.7640	0.9981

As the pH increases from 7.71 to 8.52, the yield stress decreases by approximately 10.45 %, the consistency index K decreases by 43.54 %, and the flow index n increases by 14.79 %, indicating less pronounced shear-thinning behavior at higher pH.

Figure 5 shows shear stress at a fixed shear rate ($\dot{\gamma}$ = 83.3 s^{-1}) as a function of pH, with the point of zero charge (p.z.c. = 7.85) indicated by the red vertical line. The shear stress is maximum near the p.z.c. and decreases monotonically as it moves away from this critical value, approaching an asymptotic minimum for pH ≥ 8.3.

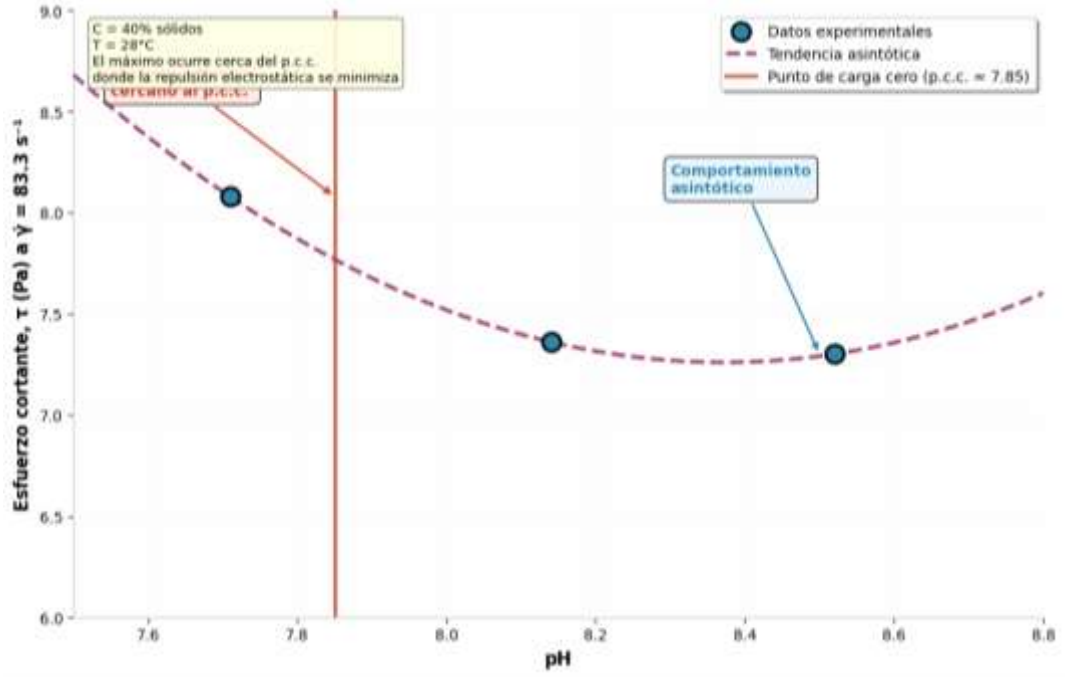


Figure 5. Shear stress at $\dot{\gamma}$ = 83.3 s^{-1} as a function of pH (C = 40 %).

This behavior reflects the influence of surface charge on interparticle forces. Near the p.z.c., electrostatic repulsion is minimized, allowing van der Waals

attractive forces to dominate and promote flocculation (Cardero and Garcell, 2016; Pérez-García and Garcell-Puyáns, 2017). Flocculated structures increase resistance to flow, manifested as higher yield stress and apparent viscosity. As the system moves away from the p.z.c., surface charge develops, generating electrostatic repulsion, dispersing particles, reducing flocculation, and decreasing resistance to flow. The asymptotic behavior for pH ≥ 8.3 suggests that, once a certain magnitude of surface charge has been reached, further increases produce diminishing returns in interparticle repulsion, consistent with DLVO theory (Hernández-Ramírez, 2017; Pérez-García and Garcell-Puyáns, 2017).

To resolve the pH-rheology versus pH-neutralization dilemma, it should be considered that although pH significantly influences the Herschel-Bulkley parameters, its role as a process variable should be reassessed. The neutralizing function of the slurry is determined by the mass flow of $CaCO_3$ and its specific surface area, not by the pH of the suspension at which it is transported before neutralization. Therefore, it is recommended to operate the slurry at pH ≥ 8.3 to minimize flow resistance, adjusting the slurry flow rate according to the neutralization demand, which has a positive impact on the energy efficiency of the pumping system.

3.2.3. Influence of polydispersity

The polydispersity index (s), inversely related to distribution width, shows systematic correlations with the rheological parameters. Figure 6 presents three-dimensional visualizations of the dependence of τ_0, K, and n on C and s at pH = 8.14. These results are consistent with those reported by Martínez-Rojas *et al.* (2026), since they correspond to the same slurry. However, the analysis proposed here focuses on demonstrating the Herschel-Bulkley behavior of carbonate sludge on the basis of the three-dimensional dependence of the rheological parameters on the operating variables considered. This aspect differs from the previous work by the lead author, in which the analysis was used to validate the empirical correlations developed.

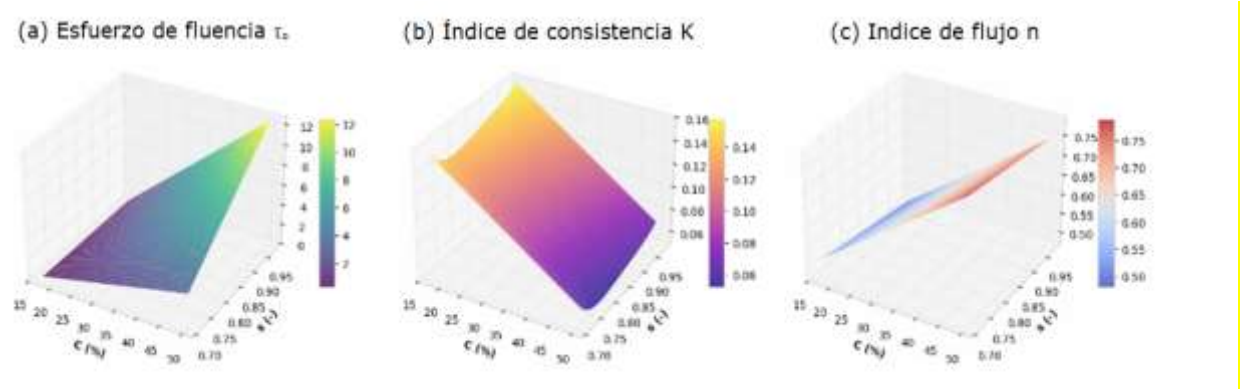


Figure 6. Dependence of the Herschel-Bulkley parameters (τ_0, K, and n) on C and s at pH = 8.14 (adapted from Martínez-Rojas *et al.*, 2026).

The yield stress τ_0 increases with both C and s (Figure 6a). The increase with s indicates that narrower distributions (higher s) produce higher τ_0 at equivalent concentrations because monodisperse systems do not achieve the efficient packing of polydisperse systems, thereby increasing interparticle contact and network formation (Hernández-Ramírez *et al.*, 2016; Pérez-García and Garcell-Puyáns, 2017). The consistency index K exhibits a nonmonotonic dependence on s (Figure 6b): at low s (broad distributions), K decreases as s increases; at high s (narrow distributions), K increases with s. This reflects competing mechanisms: improved packing reduces hydrodynamic interactions (decreasing K), whereas increased interparticle contacts strengthen the network (increasing K), with an equilibrium around s ≈ 0.8. The flow index n decreases as s increases (Figure 6c), indicating that narrower distributions produce more pronounced shear-thinning behavior, consistent with studies in colloidal systems (Luckham and Ukeje, 1999). Monodisperse systems form stronger particle networks that break down more dramatically under shear, which is related to the enlargement of interparticle contact structures in dense systems (Goyal *et al.*, 2024).

3.3. Model comparison: Bingham vs. Herschel-Bulkley

To quantitatively justify the transition from the Bingham classification to the Herschel-Bulkley classification, both models were fitted to each experimental flow curve. Table 6 presents comparative statistics for representative samples at different concentrations.

Table 6. Comparison of Bingham and Herschel-Bulkley model fits

C (%)	Bingham R^2	H-B R^2	AIC (Bingham)	AIC (H-B)	F statistic	p-value
17.41	0.9823	0.9981	-23.4	-31.7	18.2	0.003
30.16	0.9765	0.9968	-18.7	-28.3	22.5	0.001
39.90	0.9682	0.9963	-15.2	-26.8	27.1	<0.001
49.86	0.9527	0.9958	-11.3	-24.2	32.8	<0.001

For all samples, the Herschel-Bulkley (H-B) model provides a superior fit, as indicated by higher R^2 values and lower AIC scores. The F-test for nested models (Bingham as a particular case of H-B with n = 1) yields p-values < 0.005 for all concentrations, rejecting the null hypothesis that the Bingham model is adequate. The improvement in fit becomes more pronounced as concentration increases: the difference in R^2 rises from 0.0158 at 17 % to 0.0431 at 50 % solids. This trend reflects the increasing importance of nonlinear post-yield behavior at higher concentrations, where particle networks generate more complex stress-strain relationships, consistent with studies in concentrated colloidal suspensions (Sutherland *et al.*, 2015; Pérez-García and Garcell-Puyáns, 2017).

Figure 7 illustrates the comparison for a representative sample (C = 40 %, pH = 8.14). The Herschel-Bulkley model captures the curvature of the flow curve, whereas the Bingham model enforces linearity, overpredicting shear stress at intermediate shear rates and underpredicting it at high shear rates.

The systematic deviations of the Bingham model have practical implications for pipeline transport. Overprediction of shear stress at intermediate shear rates would overestimate pressure drop under typical operating ranges, whereas underestimation at high shear rates could underestimate pumping requirements during high-flow conditions (Narayanan *et al.*, 2024; Whorton *et al.*, 2025).

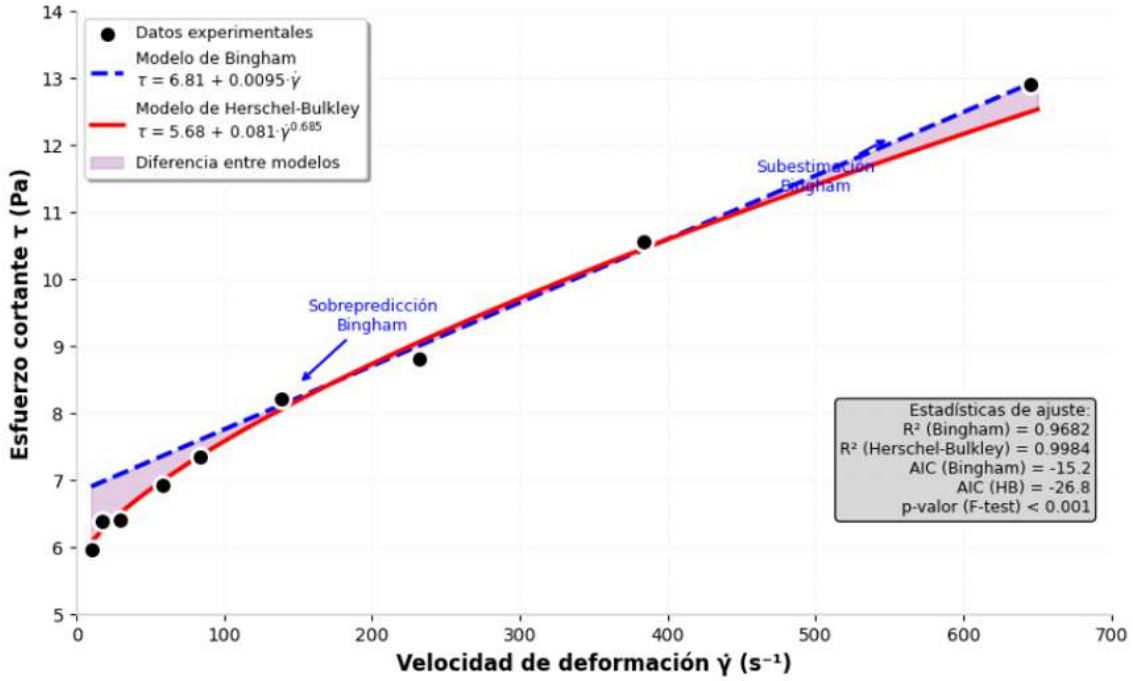


Figure 7. Comparison of Bingham and Herschel-Bulkley fits for C = 40 %, pH = 8.14. Symbols: experimental data. Dashed line: Bingham fit. Continuous line: Herschel-Bulkley fit.

3.4. Empirical correlations for Herschel-Bulkley parameters

For engineering applications requiring rapid estimates of rheological parameters, Martínez-Rojas *et al.* (2026) developed empirical correlations from the operating variables (C, pH, and s) described in Section 2.2.

3.4.1. Yield stress (τ_0)

Multiple regression analysis produced the following correlation for yield stress (Equation 5):

$$\tau_0 = 11{,}734 - 0{,}17124C - 0{,}10854pH - 24{,}259s - 0{,}05679 \cdot (C \times pH) + 1{,}0253 \cdot (C \times s) + 0{,}86935 \cdot (pH \times s) \quad (5)$$

The correlation presents $R^2 = 0.9984$ and a standard error of 0.160 Pa, with all coefficients statistically significant ($p < 0.001$), and is valid within the experimental ranges: $17 \leq C \leq 50$ %, $7.71 \leq pH \leq 8.52$, and $0.713 \leq s \leq 0.985$. The interaction terms capture nonadditive effects; the positive C×s interaction indicates that polydispersity amplifies the effect of concentration, consistent with the fact that narrower distributions enhance network formation at high concentrations.

3.4.2. Consistency index (K)

The consistency index K required a more complex functional form because of its nonmonotonic dependence on the variables (Equation 6):

$$K = 6085{,}74 - 0{,}002667C - 0{,}51637pH + 3549{,}38s + 0{,}50895(pH \times s) - 30726{,}16s^{0.25} + 47905{,}11s^{0{,}45} - 26813{,}80s^{0{,}65} \quad (6)$$

with R^2 = 0.9851 and a standard error of 0.0254 Pa·s^n. The terms involving fractional powers of s capture the nonmonotonic dependence on polydispersity discussed in Section 3.2.3.

3.4.3. Flow index (n)

The flow index showed the simplest functional dependence (Equation 7):

$$n = -0{,}64571 + 0{,}008140C + 0{,}14172pH - 0{,}17309s \quad (7)$$

with R^2 = 0.9216 and a standard error of 0.0267. The positive coefficient for C indicates that n increases with concentration up to the transition point, whereas the negative coefficient for s reflects the tendency toward more pronounced shear-thinning behavior in monodisperse systems.

3.4.4. Apparent viscosity (μ_a)

For the characteristic shear rate of the industrial process ($\dot{\gamma}$ = 231 s^{-1}), the apparent viscosity was correlated by Equation 8, obtained as an original result of the present work:

$$\mu_a = -0{,}08459 - 0{,}0001614C - 0{,}008078pH + 0{,}23288s \quad (8)$$

with R^2 = 0.9964 and a standard error of 0.00138 Pa·s. The simplicity of this correlation reflects the linearizing effect of high shear rates on the flow curve.

3.5. MODEL VALIDATION

3.5.1. Internal validation

The empirical correlations were validated using the original dataset through cross-validation. Table 7 presents prediction errors for representative samples.

The mean absolute errors for all parameters remain below 4.38 %, confirming the high predictive accuracy of the empirical correlations developed (Equations 6, 7, 8, and 9) within the experimental range investigated (C = 17 %-50 %, pH = 7.71-8.52, s = 0.713-0.985).

Table 7. Experimental validation of the model

Parameter	**C = 40% pH = 8.14 s = 0.846**	**C = 30% pH = 7.71 s = 0.764**	**C = 45% pH = 8.52 s = 0.908**
τ_0 (Pa)			
Experimental	4.8807	3.1824	6.6556
Predicted	4.7652	3.2451	6.8123
Error (%)	2.37	1.97	2.35
K (Pa·s^n)			
Experimental	0.1660	0.0746	0.2641
Predicted	0.1642	0.0761	0.2598
Error (%)	1.08	2.01	1.63
n (adimensional)			
Experimental	0.5902	0.6578	0.5431
Predicted	0.5987	0.6489	0.5512
Error (%)	1.44	1.35	1.49
μ_a (Pa·s) a $\dot{\gamma}$ = 231 s^{-1}			
Experimental	0.0398	0.0251	0.0509
Predicted	0.0402	0.0262	0.0508
Error (%)	1.01	4.38	0.20

3.5.2. Comparison with literature data

Figure 8 compares the experimental results of this work with literature data for calcium carbonate suspensions and similar systems. The data from Pérez-García *et al.* (2010) for lateritic suspensions at comparable concentrations fall within the scatter of the measurements in the present study, whereas the predictions of the Bingham model by Martínez-Rojas and Hernández-Ramírez (2015) deviate systematically at high shear rates.

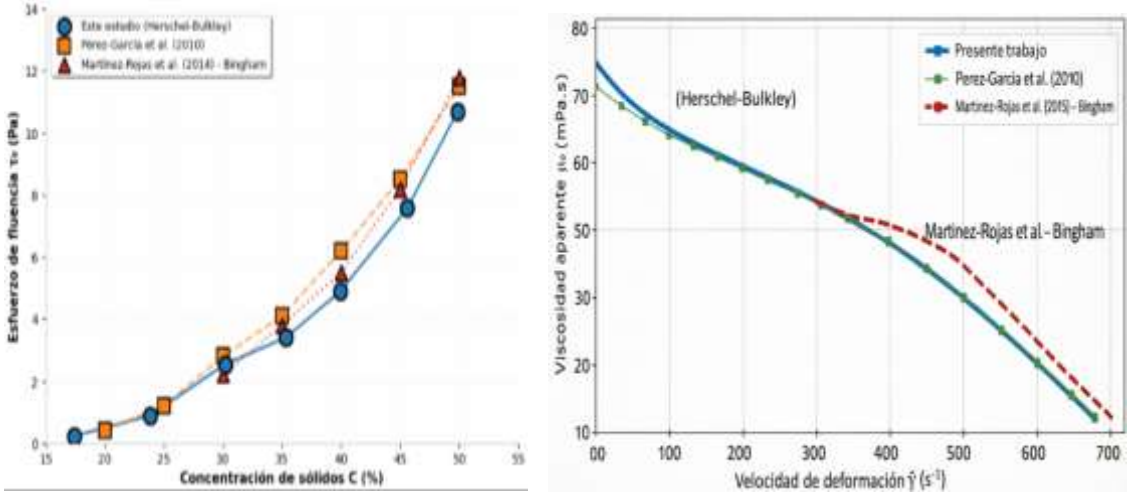


Figure 8. Comparison of experimental results with literature data.

The good agreement with independent datasets confirms that the Herschel-Bulkley characterization captures the essential rheological features of carbonate sludge slurries across different sample origins and preparation methods.

3.6. Implications for pipeline transport

The transition from Bingham to Herschel-Bulkley characterization has significant implications for pipeline-transport calculations. For laminar flow of Herschel-Bulkley fluids in circular pipes, the pressure gradient is given by Equation 10 (Visintainer *et al.*, 2023):

$$\frac{\Delta P}{L} = \frac{4}{D}\left[\tau_0 + K\left(\frac{3n+1}{4n}\right)^n \left(\frac{32Q}{\pi D^3}\right)^n\right] \quad (10)$$

where D is the pipe diameter (m), Q is the volumetric flow rate (m^3/h), ΔP/L is the head loss or pressure gradient (Pa/m), and L is the length (m).

Using the Bingham model (n = 1) would simplify the equation to Equation 11:

$$\frac{\Delta P}{L}\Big|_{Bingham} = \frac{4}{D}\left[\tau_0 + K\left(\frac{32Q}{\pi D^3}\right)\right] \quad (11)$$

Table 8 presents the results of the head-loss calculation for each concentration, together with the absolute and relative difference between the two models.

Table 8. Comparison of head loss between the Herschel-Bulkley and Bingham models under typical industrial conditions (Q = 0.03 m³/s; D = 0.1 m; C = 40 %; pH = 8.14)

Concentration C (%)	ΔP/L Herschel-Bulkley (Pa/m)	ΔP/L Bingham (Pa/m)	Absolute difference (Pa/m)	Relative overestimation (%)
30	104.32	117.81	13.49	12.9
40	200.66	245.96	45.30	22.6
50	436.08	615.32	179.24	41.1

The results in Table 8 reveal a clearly defined trend: the overestimation of head loss by the Bingham model increases significantly with solids concentration. For C = 30 %, the relative overestimation is 12.9 %; at C = 40 % (typical industrial condition), it reaches 22.6 %; and at C = 50 %, where the difference becomes critical, the Bingham model overestimates head loss by 41.1 % relative to the Herschel-Bulkley model.

4. CONCLUSIONS

- Carbonate sludge slurries exhibit viscoplastic behavior described by the Herschel-Bulkley model ($R^2 > 0.99$) over the entire experimental range (C = 17 %-50 %, pH = 7.71-8.52, $\dot{\gamma}$ = 10-650 s^{-1}), surpassing the previous Bingham classification, especially at high solids concentrations.

- The yield stress (τ_0) presents two regimes with a critical transition at C ≈ 30 %: below this value it increases moderately; above it, it grows exponentially, evidencing the formation of a percolated particle network.

- The rheological parameters depend systematically on pH, with maxima at the point of zero charge (p.z.c. ≈ 7.7-8.0). For pH > p.z.c., τ_0 and K decrease asymptotically while n increases, indicating stronger electrostatic repulsion and lower flocculation.

- The polydispersity index (s = 0.749-0.976; s > 0.7) significantly influences the rheological behavior of the investigated slurry: higher s values (narrower distributions) increase τ_0 and the shear-thinning character at equal solids concentration through more efficient formation of percolated networks.

- The discrepancy in predicted pressure drop between the Herschel-Bulkley and Bingham models is notable and increases with slurry solids

concentration (C): 12.9 % at C = 30 % and 41.1 % at C = 50 %. The Bingham model consistently overestimates pressure drop, affecting pump sizing, energy consumption, and operating decisions. Adoption of the Herschel-Bulkley model as the standard for designing pipelines transporting this type of suspension improves process efficiency.

Taken together, these results contribute to understanding the rheology of carbonate sludge slurries and provide a theoretical-experimental basis for engineering calculations in the Cuban nickel industry and other applications involving carbonate suspensions.

5. REFERENCES

Abbasi Moud, A., Poisson, J., Hudson, Z. M., & Hatzikiriakos, S. G. (2021). Yield stress and wall slip of kaolinite networks. *Physics of Fluids*, *33*(5), 053105. https://doi.org/10.1063/5.0050541

ASTM. (2010). *Standard test methods for rheological properties of non-Newtonian materials by rotational (Brookfield type) viscometer* (ASTM D2196-10). ASTM International. https://store.astm.org/d2196-05.html

Boyer, F., Guazzelli, É., & Pouliquen, O. (2011). Unifying suspension and granular rheology. *Physical Review Letters, 107*(18), 188301. https://doi.org/10.1103/PhysRevLett.107.188301

Cardero, Y., & Garcell, L. R. (2016). Ionic potential effect on specific absorption cation suspensions and silt laterite carbonated. *Chemical Technology*, *30*(3), 78-86. https://tecnologiaquimica.uo.edu.cu/index.php/tq/article/view/1012

Carotenuto, C., Vananroye, A., Vermant, J., & Minale, M. (2015). Predicting the apparent wall slip when using roughened geometries: A porous medium approach. *Journal of Rheology, 59*(5), 1131. https://doi.org/10.1122/1.4923405

Carravetta, A., Fecarotta, O., Martino, R., & Sabatino, C. (2020). Assessment of rheological characteristics of a natural Bingham-plastic mixture in turbulent pipe flow. *Journal of Hydraulic Engineering, 136*(10). https://doi.org/10.1061/(ASCE)HY.1943-7900.0000239

Chhabra, R. P., & Richardson, J. F. (2008). *Non-Newtonian Flow and Applied Rheology: Engineering Applications* (2nd ed.). Butterworth-Heinemann. ISBN: 0080951600, 9780080951607. https://doi.org/10.1016/B978-0-7506-8532-0.X0001-7

Coussot, P. (2014). *Rheophysics: Matter in all its states*. Springer. https://doi.org/10.1007/978-3-319-06148-1

Derakhshan, A., Shojaei, A., & Sadeghi, M. (2023). Rheology of non-Brownian suspensions: a rough contact story. *Rheologica Acta, 62*(5-6), 1-16. https://doi.org/10.1007/s00397-023-01394-z

Geri, M., Saint-Michel, B., Divoux, T., McKinley, G. H., & Manneville, S. (2024). Interplay between wall slip and shear banding in a thixotropic yield stress fluid. *Soft Matter, 20*(29), 5769-5780. https://doi.org/10.1039/D4SM00226A

Goyal, A., Martys, N. S., & Del Gado, E. (2024). Flow induced rigidity percolation in shear thickening suspensions. *Journal of Rheology, 68*(2), 219-228. https://doi.org/10.1122/8.0000786

Hernández-Ramírez, G. (2017). *Modelación de los parámetros reológicos de las pulpas lateríticas y su influencia en el sistema de bombeo*. (Tesis doctoral, Instituto Superior Minero Metalúrgico, Cuba). https://doi.org/10.13140/RG.2.2.18732.78721

Hernández-Ramírez, G., Legrá-Lobaina, A., Garcell-Puyáns, L., & Martínez-Rojas, R. (2016). Evaluación de un modelo de polidispersión para la caracterización granulométrica de la pulpa laterítica y el cieno carbonatado. *Minería y Geología, 32*(3), 47-59. https://revista.ismm.edu.cu/index.php/revistamg/article/view/art4_No3_2016

Hernández-Rodríguez, M., Peña-Betancourt, F., & Gonzáles-Griggs, L. (2015). Analysis Benefit Process of Carbonated Silt. *Chemical Technology*, *36*(1), 69-84. https://tecnologiaquimica.uo.edu.cu/index.php/tq/article/view/597

Hopmann, C., Nillius, U., Leuchtenberger-Engel, L., & Limper, A. (2025). Measurement of wall shear stress for identification of wall slip effects in rubber compounds. *Kautschuk, Gummi, Kunststoffe: KGK, 78*(4), 35-41. https://www.kgk-rubberpoint.de/e-paper/

Hunter, R. J. (2001). *Foundations of colloid science*. Second ed. Clarendon Press, Oxford. 806 p. ISBN 0-19-850502-7. https://archive.org/details/foundationsofcol0000hunt

Leong, Y. K., Boger, D. V., & Parris, D. (1991). Surface chemistry and rheological properties of zirconia suspensions. *Journal of Rheology, 35*(1), 149-165. https://doi.org/10.1122/1.550210

Luckham, P. F., & Ukeje, M. A. (1999). Effect of particle size distribution on the rheology of dispersed systems. *Journal of Colloid and Interface Science, 220*(2), 347-356. https://doi.org/10.1006/jcis.1999.6515

Martínez-Rojas, R., & Hernández-Ramírez, G. (2015). Caracterización reológica de las pulpas de cieno carbonatado. *Minería y Geología, 31*(4), 70-83. https://revista.ismm.edu.cu/index.php/revistamg/article/view/1015

Martínez-Rojas, R., Legrá-Lobaina, A. A., Ruiz-Chavarría, G., & Garcell-Puyáns, L. R. (2026). Empirical model for predicting the rheological properties of carbonated slime pulps. *Fluids*, *11*(2), 47. https://doi.org/10.3390/fluids11020047

Minale, M. (2013). On the use of rough geometries in rheometry. *Journal of Non-Newtonian Fluid Mechanics, 199*, 30-40. https://doi.org/10.1016/j.jnnfm.2013.05.003

Mityukov, A. V., Govorov, V. A., Malkin, A. Y., & Kulichikhin, V. G. (2021). Rheology of Highly Concentrated Suspensions with a Bimodal Size Distribution of Solid Particles for Powder Injection Molding. *Polymers, DOI:10.3390/polym13162709*

Mullineux, G. (2008). Non-linear least squares fitting of coefficients in the Herschel-Bulkley model. *Applied Mathematical Modelling, 32*(12), 2538-2551. https://doi.org/10.1016/j.apm.2007.09.010

Narayanan, C., Singh, J. S., Nauer, S., Belt, R. J., Palermo, T., & Lakehal, D. (2024). Turbulent flow of non-Newtonian fluid in rough channels. *Journal of Fluid Mechanics, 1000*, A55. https://doi.org/10.1017/jfm.2024.891

Ness, C., Seto, R., & Mari, R. (2022). The physics of dense suspensions. *Annual Review of Condensed Matter Physics, 13*(1), 97-117 https://doi.org/10.1146/annurev-conmatphys-031620-105938

Pérez-García, L. (2010). *Modelo matemático que correlaciona los principales factores de influencia sobre el comportamiento reológico de las pulpas lateríticas*. (Tesis doctoral, Universidad de Oriente, Santiago de Cuba).

Pérez-García, L., & Garcell-Puyáns, L. (2006). Influencia de la distribución de tamaño de las partículas y de la temperatura sobre la reología de suspensiones lateríticas. *Tecnología Química, 26*(1), 88-93. https://www.redalyc.org/articulo.oa?id=445543749012

Pérez-García, L., & Garcell-Puyáns, L. R. (2017). Caracterización coloide-química y reológica de suspensiones acuosas de cieno carbonatado. *Tecnología Química, 37*(3). https://www.redalyc.org/journal/4455/445552858009/html/

Pérez-García, L., Garcell-Puyáns, L., Rojas-Purón, A. L., & Simões, R. (2010). Mineralogía y reología de suspensiones minerales del proceso de lixiviación ácida a presión en Moa, Cuba. *Minería y Geología, 26*(4), 16-35. https://revista.ismm.edu.cu/index.php/revistamg/article/view/60?articlesBySameAuthorPage=1

Piette, J. H., Jia, X., & Hatzikiriakos, S. G. (2024). Coupling slip and thixotropy to model the transient rheological behaviour of kaolinite suspensions. *Rheologica Acta, 63*(8), 453-468. https://ui.adsabs.harvard.edu/abs/2024AcRhe..63..615P/abstract

Slatter, P. T. (1997). The rheological characterisation of sludges. Water Science and Technology, 36(11), 9-18. https://doi.org/10.1016/S0273-1223(97)00663-X

Sutherland, A. V., Haldenwang, R., Chhabra, R., & van den Heever, E. (2015). Statistical comparison of non-Newtonian laminar and turbulent pipe flow pressure drop prediction models for sludges. In 17th International Conference Transport & Sedimentation of Solid Particles. Delft, The Netherlands.

Visintainer, R., Matousek, V., Pullum, L., & Sellgren, A. (2023). *Slurry transport using centrifugal pumps.* Springer Nature. ISBN: 978-3-031-12540-1.https://www.vista.gov.vn/vn-uploads/newbook/2024_10/slurry-transport-using-centrifugal-pumps.pdf

Wagner, N. J., & Mewis, J. (2021). Suspensions of Soft Colloidal Particles. In *Theory and Applications of Colloidal Suspension Rheology*. Cambridge University Press. https://doi.org/10.1016/j.earscirev.2025.105226

Whorton, J., Jones, T., & Wilson, L. (2025). Mudflow rheology: A review and analysis for Earth and planetary science disciplines. *Earth-Science Reviews, 270*, 105226. https://doi.org/10.1016/j.earscirev.2025.105226

Wilson, K. C., Addie, G. R., Sellgren, A., & Clift, R. (2020). *Slurry transport using centrifugal pumps.* 4th ed. Springer. ISBN: 978-3-030-62548-6. https://doi.org/10.1007/978-3-031-25440-6

Yusufi, B. K., Kapelan, Z., & Mehta, D. (2025). Advances in modeling the flow of Herschel–Bulkley fluids in pipes: A review. *Physics of Fluids* 37, 021302 https://doi.org/10.1063/5.0252248

Additional information

Conflict of interest

The authors declare that there are no conflicts of interest.

Author contributions

RMR: literature review; design and writing of the proposed article; formalization of the models; analysis of results; drafting of the article; and critical review of its content. RMR, LRGP, AALL, YRM, and GRC: general conception and execution of the research, mathematical analysis of the object of study and formalization of the models, writing and critical review of the initial manuscript version. YRM, HLLA, AALL, and JLRDC: analysis of results. YRM, JLRDC, HLLA, LRGP, GHR, and GRC: bibliographic search and analysis of results. All authors participated in writing, critical review, and approval of the final version of the manuscript.

Funding:

This research received funding from projects PS104HO001-057 and PS104HO001-075 of the program "Comprehensive Use of Mineral Resources in the Cuban Nickel Industry (PS104HO001-001)". It was also funded by projects PS223LH001-047 and PS223LH001-060 of the program "Higher Education and Sustainable Development (PS223LH001)".

ORCID

RMR, https://orcid.org/0000-0002-6846-1183

AALL, https://orcid.org/0000-0002-4793-4754

LRGP, https://orcid.org/0000-0001-6740-8017

GHR, https://orcid.org/0000-0002-5920-8311

HLLA, https://orcid.org/0000-0003-2688-015X

JLRD, https://orcid.org/0009-0003-7561-0479

GRC, https://orcid.org/0000-0002-7553-0730

YRM, https://orcid.org/0000-0002-5098-5675

Received: 29/04/2026

Accepted: 11/05/2026